Australian Earthquake Engineering Society
2022 National Conference, 24-25 November 2022
Mount Macedon, Victoria, Australia

A novel tuned negative stiffness inerter damper for structural vibration control under earthquakes

Huan Li, Kaiming Bi* and Hong Hao

Centre for Infrastructure Monitoring and Protection, School of Civil and Mechanical Engineering, Curtin University, Kent Street, Bentley, WA 6102, Australia

Corresponding author: Kaiming.Bi@curtin.edu.au

Abstract

In this paper, a novel tuned negative stiffness inerter damper (TNSID) that is made by combining the advantages of negative stiffness, inerter, and tune effect is proposed for effective structural seismic protection. The realisation and fundamentals of the TNSID are introduced with mechanical property analyses, which demonstrate that the TNSID can achieve the required magnitude of negative stiffness and significant mass amplification effect through amplification mechanisms. By minimising its maximum displacement amplification factor, the closed-form expressions of the optimal structural parameters of the TNSID are obtained based on the equal-peak method. The performance of the proposed TNSID in structural vibration control is evaluated on a single-degree-of-freedom (SDOF) structure subjected to different excitations. Comparative studies are made among the system without control, with TNSID, tuned viscous mass damper, tuned inerter damper and negative stiffness amplifying damper. The analytical results show that the TNSID is capable of mitigating the displacement and acceleration responses simultaneously. Compared to the devices consisting of either inerter or negative stiffness, the TNSID can achieve the lowest displacement and acceleration responses and the widest effective frequency bandwidth.

Keywords: Negative stiffness, Inerter, Seismic protection, Structural vibration control

1 Introduction

Due to the advantages of high reliability, no energy consumption, simple design and low maintenance cost, the passive vibration control strategies have been extensively investigated and widely applied to protecting engineering structures from harmful vibrations (Spencer Jr and Nagarajaiah 2003). By and large, passive vibration control devices can be categorised into energy dissipators, vibration isolators and dynamic vibration absorbers (Mosqueda et al. 2004, De Domenico and Ricciardi 2018, Zuo et al. 2021).

Negative stiffness element (NSE) has attracted great research interests in the field of both mechanical and civil engineering recently, which has been verified to be especially effective for low and ultra-low frequency vibration control. To date, different realisations of NSE have been developed. Li et al. (2020) recently provided a comprehensive review of the NSE-based vibration control techniques. By combining NSEs with other elements, such as damping and positive stiffness elements, a series of NSE-based vibration control devices have been

developed and investigated, including negative stiffness damper, negative stiffness amplification dampers (NSADs), KDampers and negative stiffness dynamic vibration absorbers (Sarlis et al. 2012, Shen et al. 2017, Wang et al. 2019, Kapasakalis et al. 2020), etc.

Inerter has also been verified effective for structural vibration control. As a novel passive vibration control device, the force of an inerter is proportional to the relative acceleration between its two terminals (Smith 2002). It can generate an inertance that is thousands of times its physical mass, which thereby has the capacity to address the issue of traditional vibration absorbers that require a large physical mass to produce sufficient control force. In general, the inerter can be further divided into different categories and a comprehensive review has been presented by Ma et al. (2021) recently. By combining the inerter with damper, spring and physical mass elements, researchers have proposed various inerter-based vibration control devices with different configurations, such as tuned viscous mass dampers (TVMDs), tuned inerter dampers (TIDs) and inertial mass dampers, etc (Ikago et al. 2012, Lazar et al. 2014, Lu et al. 2017).

Although previous studies revealed that both the NSE- and inerter-based vibration control devices generally outperform the conventional passive vibration control devices, they both have specific limitations. For example, introducing negative stiffness results in stiffness reduction of the entire system, which may lead to instability problems (Shi and Zhu 2019). Due to its force being a function of the square of vibration frequency (Smith 2002), the inerter may apply excessive force to the structure under high-frequency excitation while it may become ineffective under low-frequency excitation. One of the promising potentials to overcome the above issues and obtain better vibration control performance is to develop a system that integrates both NSE and inerter. To the best knowledge of the authors, only very limited studies have been carried out in this area. Wang et al. (2019) combined the NSE with four kinds of inerter-based vibration control devices and compared their vibration control performance on a single-degree-of-freedom (SDOF) structure. It was demonstrated that, compared to their counterparts, the integrated devices could attain lower displacement transmissibility and wider effective frequency bandwidth. By combining NSE, inerter, positive stiffness and damping elements, Wang et al. (2021) developed a tuned negative stiffness inerter damper (TNSID), which was verified to be more effective and robust than TID and TVMD. Based on the same elements, Ye and Nyangi (2020) proposed a TNSID with different configurations and implemented it onto a five-storey building structure. However, most of these studies were based on the mechanical model without considering the physical realisations of the TNSID, as well as the cooperation of the NSE and inerter. Furthermore, the fundamentals of the TNSID and the effects of its NSE and inerter elements in structural vibration control have not been fully studied.

In this paper, to address the challenges mentioned above and fill the gaps of knowledge, a novel TNSID is proposed. The realisations and fundamentals of the TNSID are introduced in Section 2. The related mathematical equations and the expressions of its optimal parameters are given in Section 3. Following that, in Section 4, the TNSID is implemented onto a SDOF structure to evaluate its vibration control performance. The results are analysed and compared with the other three commonly used devices, including TID, TVMD and NSAD. Finally, the concluding remarks are drawn in Section 5.

2 Working mechanism of the TNSID

Figure 1 (a) and (b) show the schematic and the mechanical model of a SDOF structure with the proposed TNSID. The TNSID (i.e., shown in the pink dash box) in the present study is composed of the combined NSE and inerter component (i.e., shown in the blue dash box), positive stiffness elements and conventional dashpots. As depicted in Figure 2(a), the

combined NSE and inerter component of the TNSID consists of eight parts, including (1) the chevron-braced frame, (2) the pre-stretched springs, (3) the vertical lever arm, (4) the spring support rod, (5) the rod arm, (6) the horizontal lever arm, (7) the leverage pivot on the bottom plate and (8) the lumped mass. Among these eight parts, the combined use of parts (1)-(5) can achieve negative stiffness, i.e., form the NSE, while parts (1), (3), (5) and (6)-(8) consist of the inerter component to attain significant mass amplification effect. The bottom of the chevron-braced frame is fixed onto a bottom plate by bolts, and the top of the rod arm is connected to the superstructure. The vertical lever arm can rotate around hinge point C on the chevron-braced frame, which can further promote the movement of the spring support rod, rod arm and horizontal lever arm. Two pre-stretched springs are installed on each side of the spring support rod to ensure force balance. Other ends of the pre-stretched springs are attached to the bottom plate, which can rotate around point J.

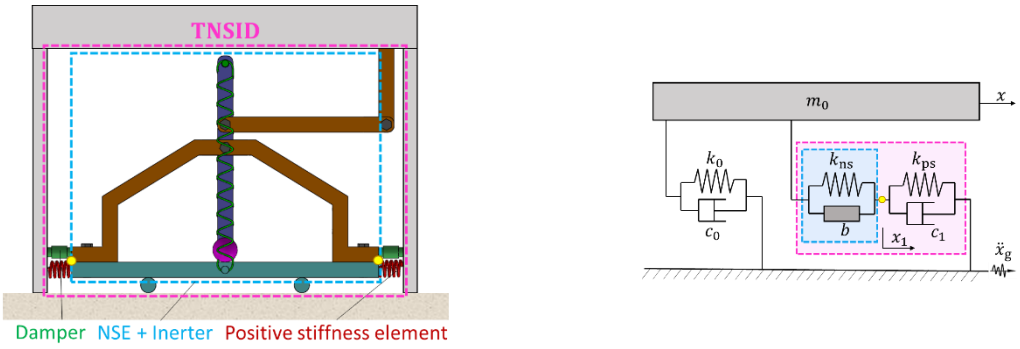

(a) Schematic of the TNSID system (b) Mechanical model of the TNSID system

Figure 1. The implementation of TNSID on a SDOF structure.

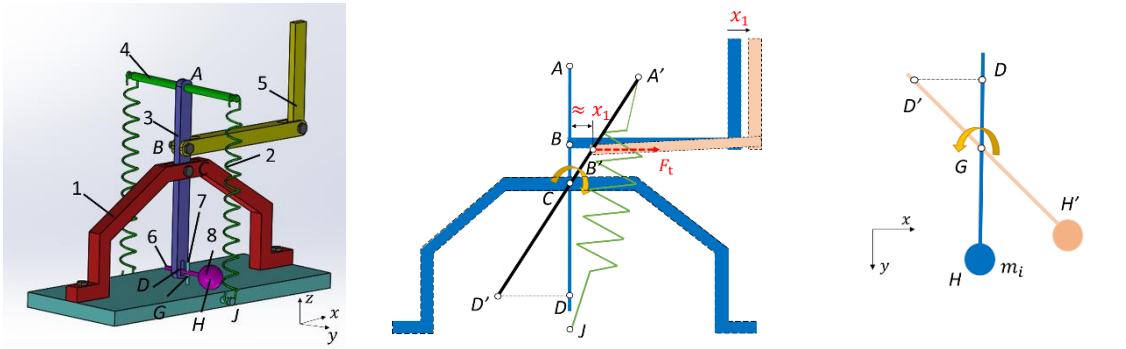

(a) Schematic of the NSE and inerter component (b) State of motion in the vertical plane (c) State of motion in the horizontal plane

Figure 2. The combined NSE and inerter component of the TNSID.

As shown in Figure 2 (b) and (c), when there is a small displacement x_1, the vertical level arm will rotate around point C clockwise, which leads to the clockwise rotation of the pre-stretched springs around point J and the anticlockwise rotation of the horizontal lever arm around point G. During this process, the pre-stretched springs release the pre-stored potential energy to pull the vertical level arm to rotate further. Since the spring force assists displacement instead of resisting it, negative stiffness is thereby generated. Furthermore, the rotational angular acceleration of the lumped mass is related to the ratios between BC and CD, as well as DG and GH, which means the TNSID can realise a two-stage mass amplification effect. According to Figure 2, the NSE and inerter components of the TNSID are connected in parallel.

3 Mathematical equation of the TNSID

Based on Figure 1(b), the equation of motion of the TNSID system can be described by

$$m_0\ddot{x} + c_0\dot{x} + k_0x + b\ddot{x}_1 + k_{\mathrm{ns}}x_1 = -m_0\ddot{x}_{\mathrm{g}} \quad (1\text{-}1)$$

$$b\ddot{x}_1 + k_{\mathrm{ns}}x_1 = k_{\mathrm{ps}}(x - x_1) + c_1(\dot{x} - \dot{x}_1) \quad (1\text{-}2)$$

in which, m_0, k_0 and c_0 are the mass, stiffness and damping coefficient of the SDOF structure, respectively; b, k_{ns}, k_{ps} and c_1 represent the inertance, negative stiffness, positive stiffness and damping coefficient of the TNSID, respectively; x, x_1 and $\ddot{x}_{\mathrm{g}}$ stand for the displacement of the structure, internal displacement of the TNSID and the ground acceleration, respectively.

Transforming Equations (1-1) and (1-2) into the Laplace domain and then substituting the following parameters $\omega_0 = \sqrt{\frac{k_0}{m_0}}$, $\xi_0 = \frac{c_0}{2m_0\omega_0}$, $\omega_1 = \sqrt{\frac{k_{\mathrm{ps}}}{b}}$, $\xi_1 = \frac{c_1}{2b\omega_1}$, $\mu = \frac{b}{m_0}$, $\alpha = \frac{\omega_1}{\omega_0}$ and $\beta = \frac{k_{\mathrm{ns}}}{k_{\mathrm{ps}}}$, one can obtain

$$s^2X + 2\xi_0\omega_0 sX + \omega_0^2X + \mu s^2X_1 + \mu\beta\alpha^2\omega_0^2X_1 = -A_{\mathrm{g}} \quad (2\text{-}1)$$

$$\mu s^2X_1 + \mu\beta\alpha^2\omega_0^2X_1 = \mu\alpha^2\omega_0^2(X - X_1) + 2\mu\alpha\xi_1\omega_0 s(X - X_1) \quad (2\text{-}2)$$

where $x = Xe^{st}$, $x_1 = X_1e^{st}$ and $\ddot{x}_{\mathrm{g}} = A_ge^{st}$; $s = j\omega$ is the complex frequency parameter and $j^2 = -1$.

According to Equations (2-1) and (2-2), the displacement amplification factor of the TNSID can be attained as follows

$$|DAF(\gamma)| = \sqrt{\frac{A_X^2 + B_X^2}{C_X^2 + D_X^2}} \quad (3)$$

where $\gamma = \omega/\omega_0$ is the frequency ratio, $A_X = \gamma^2 - \beta\alpha^2 - \alpha^2$, $B_X = -2\alpha\xi_1\gamma$, $C_X = \gamma^4 - (1 + \alpha^2 + \mu\alpha^2 + \beta\alpha^2 + 4\xi_0\xi_1\alpha)\gamma^2 + \alpha^2 + \beta\alpha^2 + \mu\beta\alpha^4$ and $D_X = 2\alpha\xi_1\gamma(1 + \mu\beta\alpha^2 - \gamma^2 - \mu\gamma^2) + 2\xi_0\gamma(\alpha^2 + \beta\alpha^2 - \gamma^2)$.

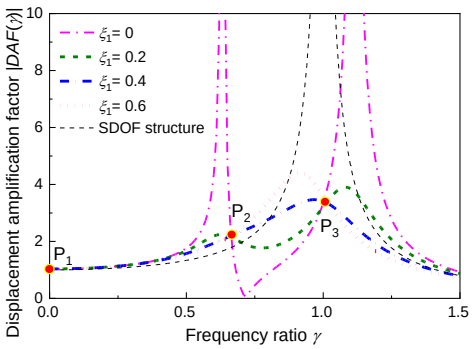

Figure 3. Displacement amplification factor curves of the TNSID under different damping ratios ξ_1 (μ =0.2, α=0.8, β=-0.2, ξ_0=0.02).

$$\alpha_{\mathrm{opt}} = \frac{1}{\sqrt{(1+\mu)^2 + \beta}} \quad (4)$$

$$\xi_{1-\mathrm{opt}} = \frac{1}{2}\sqrt{\frac{(3 + 3\mu + 3\beta + 2\mu\beta)\mu}{(2+\mu)\beta^2 + 2\beta(1+\mu)(2+\mu) + 2(1+\mu)^2}} \quad (5)$$

$$\beta_{\mathrm{opt}} = -(1+\mu)^2 + (1+\mu)\sqrt{\mu(2+\mu)} \quad (6)$$

Based on Equation (3), the displacement amplification factor curves under different damping ratios are obtained and shown in Figure 3. As can be seen, when damping ratio is 0 and 0.2, each displacement amplification factor curve has two peaks, the values of which decrease with the increment of damping ratio. Comparatively, when damping ratio increases to 0.4 and 0.6, there is only one peak on each displacement amplification factor curve, and the growth of

damping ratio will amplify the peak value. More importantly, all these curves pass through three fixed points, namely P_1, P_2 and P_3, which are independent of the damping ratio. Considering a small change of the damping ratio can result in a significant fluctuation of the displacement amplification factor of the TNSID, its parameters should be carefully optimised. In this research, based on the well-recognised fixed-point theory introduced by Den Hartog (1956), the optimal parameters of the TNSID, including the optimal frequency ratio α, damping ratio ξ_1 and negative stiffness ratio β are attained and described by Equations (4) to (6) (Wang, He et al. 2019, Ye and Nyangi 2020).

4 Performance evaluation of the TNSID

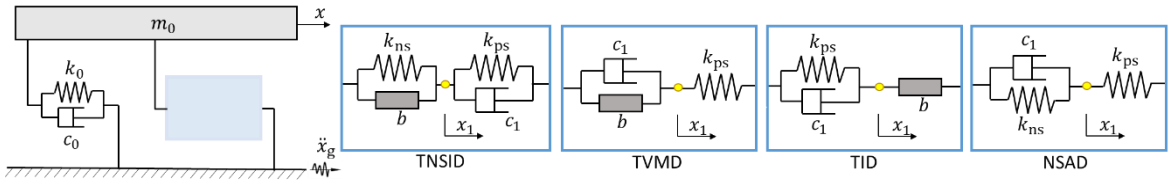

Figure 4. The analytical models of the SDOF structure with different devices.

To evaluate the feasibility and effectiveness of the proposed TNSID on structural vibration control, it is implemented onto a SDOF structure subjected to harmonic excitation and earthquake ground motion. The natural period of the primary structure is assumed as T_0=1 s and its inherent damping ratio is ξ_0=2%. The mass ratio μ of the TNSID is set to 0.2 and its frequency ratio, damping ratio and negative stiffness ratio can be calculated by Equations (4) to (6), respectively. Another three commonly used vibration control devices, including TID, TVMD and NSAD, are also investigated for comparison. As shown in Figure 4, the TID, TVMD and NSAD consist of either inerter or NSE. The closed-form expressions of their optimal parameters attained with Den Hartog's fixed-point theory have been derived and provided in previous studies (Ikago et al. 2012, Lazar et al. 2014, Wang et al. 2019). To compare their vibration control performance on a fair basis, the NSAD is designed with the same negative stiffness as the TNSID, and the TVMD and TID feature the same mass ratio as the TNSID.

4.1 Under harmonic excitation

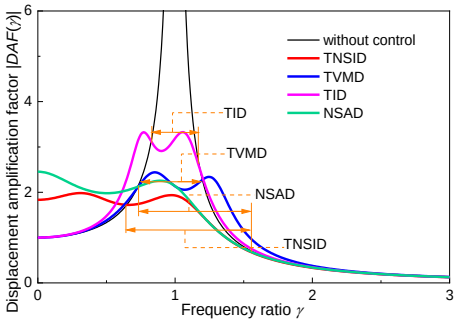

Figure 5. Displacement amplification factors of the SDOF structure with different devices ($\mu = 0.2$).

The displacement amplification factor curves of TNSID, TVMD, TID and NSAD under harmonic excitation are shown in Figure 5. Compared to the SDOF structure without control, all these four devices can significantly reduce the maximum displacement amplification factor, which validates their vibration control effect. The displacement suppression effect of the proposed TNSID is superior to the other three devices by achieving the lowest displacement response. As the orange arrows indicate, the control effectiveness of these four devices can be ranked in ascending order as TID, TVMD, NSAD and TNSID.

4.2 Under earthquake ground motions

To evaluate the seismic protection performance of these four devices, six real earthquake ground motions selected from the databases of Pacific Earthquake Engineering Research Centre and National Geophysical Data Centre are applied to the SDOF structure. The details of these six earthquake ground motions are given in Table 1.

Table 1 Information about the six earthquake ground motions.

Name	Date	Recording station	Mw	PGA(g)	Type
Cape Mendocino	1992-04-25	Fortuna	7.2	0.12	FF
Landers	1992-06-28	Coolwater	7.3	0.42	FF
Tokachi-Oki	1968-05-16	Hachinohe Harbor	7.9	0.23	FF
Kobe	1995-01-17	KJMA	6.9	0.84	NFP
Loma Prieta	1989-10-18	BRAN	6.9	0.46	NFNP
Imperial Valley-06	1940-05-18	El Centro, Array #5	6.5	0.38	NFP

* FF: far-field, NFP: near-fault with pulse, NFNP: near-fault without pulse.

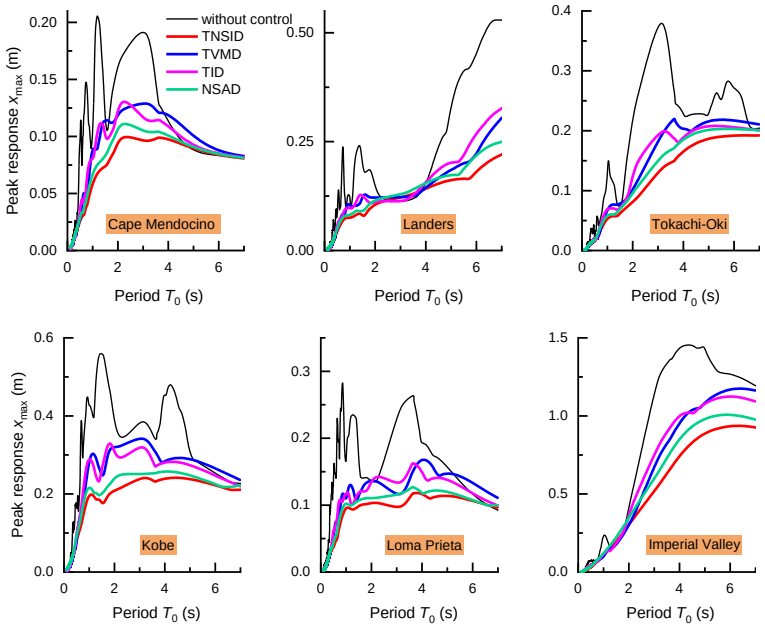

Figure 6. Peak displacement responses of the SDOF structure with different control devices under six earthquake ground motions ($\mu = 0.2$).

The peak displacement and acceleration responses of the SDOF structure with different structural periods under six earthquake ground motions are shown in Figures 6 and 7, respectively. As can be seen, these four devices can attain lower peak displacement and acceleration responses for structures with the most considered vibration periods as compared to the uncontrolled SDOF structure. Particularly, the performance of the TNSID is the most prominent among these four devices, the peak displacement and acceleration responses of which are the lowest. For instance, in Figure 6, when the structural period is 2.2 s, the peak displacement response of the structure with the TNSID under the Cape Mendocino Earthquake is 89%, 76% and 80% that of the systems with NSAD, TID and TVMD, respectively. As Figure 7 shows, for a structure with a period of 0.25s subjected to the Tokachi-Oki Earthquake, the employment of TNSID can further decrease the peak acceleration response from 0.390g (NSAD), 0.538g (TID) and 0.574g (TVMD) to 0.378g. Moreover, as demonstrated in Figure 6, by comparing the TNSID with NSAD, the addition of the inerter endows the TNSID with the capacity to attain more significant displacement control effect. Besides, both TNSID and TID are designed with inerter, while the TNSID is equipped with an additional NSE. It can be observed from Figures 6 and 7 that the displacement suppression and acceleration mitigation effects of the TNSID outperform that of the TID. The reason lies in that the NSE can amplify the deformation of the damping element in the TNSID, hence enhancing the energy dissipation capacity and displacement suppression effect.

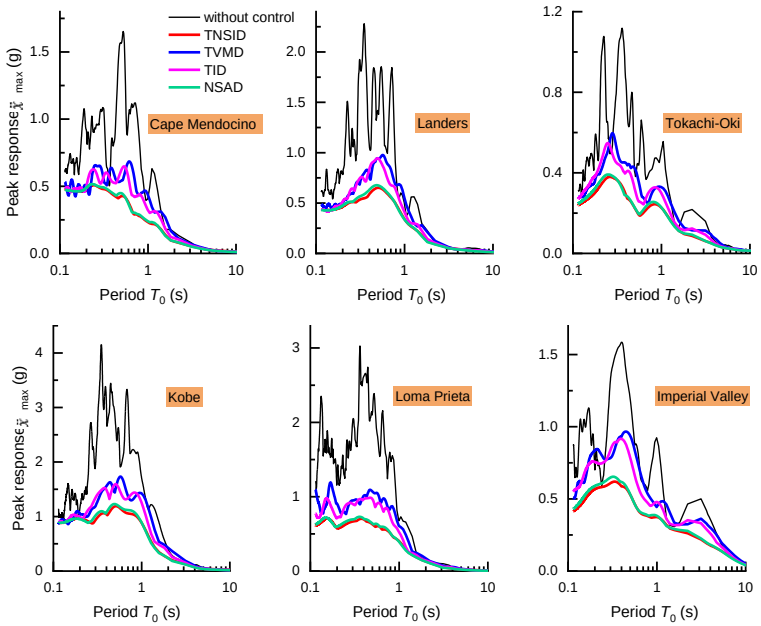

Figure 7. Peak absolute acceleration responses of the SDOF structure with different control devices under six earthquake ground motions ($\mu = 0.2$).

5 Conclusion

This paper develops a novel TNSID for effective structural vibration control, which integrates the advantages of NSE, inerter and tune effect simultaneously. The realisations and working mechanism of the TNSID are introduced, which can achieve significant mass amplification effect and negative stiffness. After obtaining its optimal parameters with Den Hartog's fixed-point theory, the TNSID is implemented onto a SDOF structure subjected to different excitations to evaluate its feasibility and effectiveness in vibration control. The analytical results under harmonic excitation validate that, by comparing with the TVMD, TID and NSAD, the TNSID can achieve the lowest displacement amplification factor and the widest effective frequency bandwidth. Besides, when the structure is subjected to real earthquake ground motions, the proposed TNSID can result in the most satisfactory vibration mitigation effects by attaining the lowest peak displacement and acceleration responses.

Acknowledgments

This work was supported by the Australian Research Council Future Fellowship [grant numbers FT200100183].

References

De Domenico, D. and Ricciardi, G. (2018). An enhanced base isolation system equipped with optimal tuned mass damper inerter (TMDI). Earthquake engineering & structural dynamics, Vol 47, No 5, pp 1169-1192.

Den Hartog, J. (1956). Mechanical Vibrations. New York: Mcgrraw Hill Nook Company. Inc.

Ikago, K., Saito, K. and Inoue, N. (2012). Seismic control of single ‐ degree ‐ of ‐ freedom structure using tuned viscous mass damper. Earthquake Engineering & Structural Dynamics, Vol 41, No 3, pp 453-474.

Kapasakalis, K. A., Antoniadis, I. A. and Sapountzakis, E. J. (2020). Performance assessment of the KDamper as a seismic Absorption Base. Structural Control and Health Monitoring, Vol 27, No 4, pp e2482.

Lazar, I., Neild, S. and Wagg, D. (2014). Using an inerter ‐ based device for structural vibration suppression. Earthquake Engineering & Structural Dynamics, Vol 43, No 8, pp 1129-1147.

Li, H., Li, Y. and Li, J. (2020). Negative stiffness devices for vibration isolation applications: A review. Advances in Structural Engineering, Vol 23, No 8, pp 1739-1755.

Lu, L., Duan, Y. F., Spencer Jr, B. F., Lu, X. and Zhou, Y. (2017). Inertial mass damper for mitigating cable vibration. Structural Control and Health Monitoring, Vol 24, No 10, pp e1986.

Ma, R., Bi, K. and Hao, H. (2021). Inerter-based structural vibration control: A state-of-the-art review. Engineering Structures, Vol 243, pp 112655.

Mosqueda, G., Whittaker, A. S. and Fenves, G. L. (2004). Characterization and modeling of friction pendulum bearings subjected to multiple components of excitation. Journal of Structural Engineering, Vol 130, No 3, pp 433-442.

Sarlis, A. A., Pasala, D. T. R., Constantinou, M., Reinhorn, A., Nagarajaiah, S. and Taylor, D. (2012). Negative stiffness device for seismic protection of structures. Journal of Structural Engineering, Vol 139, No 7, pp 1124-1133.

Shen, Y., Peng, H., Li, X. and Yang, S. (2017). Analytically optimal parameters of dynamic vibration absorber with negative stiffness. Mechanical Systems and Signal Processing, Vol 85, pp 193-203.

Shi, X. and Zhu, S. (2019). A comparative study of vibration isolation performance using negative stiffness and inerter dampers. Journal of the Franklin Institute, Vol 356, No 14, pp 7922-7946.

Smith, M. C. (2002). Synthesis of mechanical networks: the inerter. IEEE Transactions on automatic control, Vol 47, No 10, pp 1648-1662.

Spencer Jr, B. and Nagarajaiah, S. (2003). State of the art of structural control. Journal of structural engineering, Vol 129, No 7, pp 845-856.

Wang, H., Gao, H., Li, J., Wang, Z., Ni, Y. and Liang, R. (2021). Optimum design and performance evaluation of the tuned inerter-negative-stiffness damper for seismic protection of single-degree-of-freedom structures. International Journal of Mechanical Sciences, pp 106805.

Wang, M., Sun, F.-f., Yang, J.-q. and Nagarajaiah, S. (2019). Seismic protection of SDOF systems with a negative stiffness amplifying damper. Engineering Structures, Vol 190, pp 128-141.

Wang, X., He, T., Shen, Y., Shan, Y. and Liu, X. (2019). Parameters optimization and performance evaluation for the novel inerter-based dynamic vibration absorbers with negative stiffness. Journal of sound and Vibration, Vol 463, pp 114941.

Ye, K. and Nyangi, P. (2020). H∞ Optimization of Tuned inerter damper with negative stiffness device subjected to support excitation. Shock and Vibration, Vol 2020.

Zuo, H., Bi, K., Hao, H. and Ma, R. (2021). Influences of ground motion parameters and structural damping on the optimum design of inerter-based tuned mass dampers. Engineering Structures, Vol 227, pp 111422.